Calcium flux through ER-TGN contact sites facilitates cargo export

Running title: Secretory cargo sorting requires Ca^{2+} flux in ER/TGN contact sites

Bulat R. Ramazanov[1]†, Rosaria Di Martino[2]†, Abhishek Kumar[3], Anup Parchure[1], Yeongho Kim[1], Oliver Griesbeck[4], Martin A. Schwartz[1,3,5], Alberto Luini[2]†, Julia von Blume[1]†*

[1]Department of Cell Biology, Yale University School of Medicine, New Haven, CT

[2]Institute of Biochemistry and Cell Biology, National Research Council, Via Pietro Castellino 111, 80131 Naples, Italy

[3]Yale Cardiovascular Research Center, Cardiovascular Yale School of Medicine, Yale University,

[4] Max Planck Institute of Neurobiology, Martinsried, Germany

[5] Department of Biomedical Engineering, Yale University, New Haven, CT

† Authors have contributed equally to the work

*Corresponding author

Julia von Blume

333 Cedar Street

New Haven, CT 06510

USA

Yale email: julia.vonblume@yale.edu

Phone: +1 475 325 8124

Summary

The current study demonstrates that the trafficking of COMP and LyzC relies on Ca^{2+} flux between the endoplasmic reticulum (ER) and trans-Golgi Network (TGN). This process requires the activity of IP3 receptors, present in ER membranes, and depends on the integrity of the membrane contact site between these two organelles.

Abstract

Ca^{2+} influx into the trans-Golgi Network (TGN) promotes secretory cargo sorting by the Ca^{2+}-ATPase SPCA1 and the luminal Ca^{2+} binding protein Cab45. Cab45 oligomerizes upon a local Ca^{2+} influx, and Cab45 oligomers sequester and separate soluble secretory cargo from the bulk flow of proteins in the TGN. However, how this Ca^{2+} flux into the lumen of the TGN is achieved remains elusive, as the cytosol has a very low steady-state Ca^{2+} concentration. The TGN forms membrane contact sites (MCS) with the Endoplasmic Reticulum (ER), whereby the close apposition of the two organelles allows the protein-mediated exchange of molecular species such as lipids. Here we show that the TGN export of Cab45 clients requires the integrity of ER-TGN MCS and IP3R-dependent Ca^{2+} fluxes in the MCS, suggesting Ca^{2+} transfer between these organelles. Using an MCS-targeted Ca^{2+} FRET sensor module, we measure the Ca^{2+} flow in these sites in real-time. These data show for the first time that ER-TGN MCS facilitates Ca^{2+} transfer required for SPCA1-dependent cargo sorting and export from the TGN, thus solving a fundamental question in cell biology.

67 ## Introduction

68 Protein secretion is a fundamental process and facilitates the integrity and cell-cell
69 communication of multiple-tissue organisms (Uhlen et al., 2015). Secreted proteins are
70 synthesized in the Endoplasmic Reticulum (ER) and transported to the Golgi apparatus in COPII
71 coated vesicle (Barlowe and Miller, 2013; Gillon et al., 2012; Zanetti et al., 2013). Upon reaching
72 the Golgi apparatus, these cargo molecules further transit from the *cis* to trans-Golgi cisterna and
73 finally get the trans-Golgi Network (TGN) (De Matteis and Luini, 2008; Di Martino et al., 2019;
74 Guo et al., 2014; Kienzle and von Blume, 2014). At the TGN, these proteins are sorted and
75 packed into different transport carriers to reach their destination, such as the cell surface, the
76 endosomal system, or secretory granules in specialized cells (Mostov and Cardone, 1995; Stalder
77 and Gershlick, 2020; Tang, 2001).

78 Protein sorting at the TGN is a complex process involving physical features of the cargoes
79 themselves and elements of the local environment and so remains a poorly understood process
80 for many proteins. Understanding how soluble secretory proteins can be accurately sorted into
81 transport vesicles targeting the plasma membrane is challenging. No cargo receptors connect
82 these soluble molecules to the TGN membrane (Kienzle and von Blume, 2014; Pakdel and von
83 Blume, 2018; Ramazanov et al., 2021).

84 Work from us and others has shown that Calcium (Ca^{2+}) is a significant regulator of cargo
85 sorting at the TGN. The Secretory Pathway ATPase 1 (SPCA1) pumps Ca^{2+} from the cytoplasm
86 into the TGN lumen in an ATP-dependent manner (Kienzle et al., 2014; Lebreton et al., 2021;
87 Lissandron et al., 2010; Missiaen et al., 2007; Pizzo et al., 2011; Pizzo et al., 2010; Sepulveda et
88 al., 2008; von Blume et al., 2011; Wong et al., 2013). In response to luminal Ca^{2+} influx, the
89 Golgi resident protein Cab45 oligomerizes and captures cargo molecules before they are packed

90 into sphingomyelin-rich vesicles that bud from the TGN (Crevenna et al., 2016; Deng et al.,
91 2018; Scherer et al., 1996; von Blume et al., 2012). Despite the importance of Ca^{2+} in these
92 processes, the source of the Ca^{2+} pumped into the TGN lumen by SPCA1 is unknown, as the
93 cytosolic Ca^{2+} concentrations are in the low nanomolar range (Berridge et al., 2003).

94 The TGN forms MCSs with the ER, where lipids are transferred to mediate the non-
95 vesicular inter-organelle communication (Masone et al., 2019; Venditti et al., 2020; Venditti et al.,
96 2019a). Endoplasmic reticulum to TGN membrane contact sites (ER-TGN MCSs) contain
97 tethering proteins such as vesicle-associated membrane proteins A and B (VAPA and VAPB) and
98 lipid transfer proteins such as Oxysterol-binding protein 1 (OSBP1) (Lehto and Olkkonen, 2003).
99 OSBP1 possesses dual organelle targeting motifs as it can bind the ER proteins VAPA and VAPB
100 through an acidic track (FFAT) domain. It is also able to attach to the TGN through the Pleckstrin
101 homology (PH) domain, which recognizes Phosphatidylinisitol-4-phosphate (PI4P) or Arf1-GTP
102 on TGN membrane (Kawano et al., 2006; Kumagai and Hanada, 2019; Mesmin et al., 2017). At
103 the ER/TGN interface, OSBP1 counter transports PI4P from the TGN and cholesterol from the ER
104 in a process mediated by the oxysterol-binding domain (OBD) of OSBP1 that binds PI4P or
105 cholesterol in a mutually exclusive manner (Mesmin et al., 2013).

106 Recent studies report the importance of lipid transfer in ER-TGN MCSs in regulating
107 protein export from the TGN (Wakana et al., 2021). In addition to their implication in lipid transfer,
108 MCSs allow Ca^{2+} transfer between the ER and other organelles, such as the mitochondrion (Kelly,
109 1985; Pfeffer and Rothman, 1987; Rizzuto et al., 1993; Rizzuto et al., 1998). We, therefore,
110 hypothesized that ER-TGN MCSs could provide Ca^{2+} to facilitate SPCA1 and Cab45-dependent
111 cargo sorting at the TGN. Here we show that the trafficking of Cab45 clients relies on the IP3
112 receptor (IP3R), which is present in ER membranes, and on the integrity of the ER-TGN MCSs.

113 Furthermore, we generated an MCS-specific sensor to measure changes in Ca^{2+} levels within these
114 sites, revealing that this Ca^{2+} flux plays an essential role in cargo export from the TGN and depends
115 on tethering between ER and TGN. With these data, we solve a central unresolved question in cell
116 biology.

117 ## Results and discussion

118 ***Inhibition of IP3R delays TGN export of Cab45 clients***

119 Our previous work demonstrates that sorting soluble secretory proteins requires a transient
120 SPCA1-mediated Ca^{2+} influx into the TGN to facilitate Cab45 oligomerization (Crevenna et al.,
121 2016; Deng et al., 2018; von Blume et al., 2012). However, the cytosolic Ca^{2+} concentrations at
122 steady state are in the low nanomolar range and thus may not provide the amount of Ca^{2+} ions
123 required to promote the sorting of Cab45 clients (Crevenna et al., 2016; Pizzo et al., 2011). With
124 the ER being the largest Ca^{2+} store within the cell, we hypothesized that the MCS between the ER
125 and the TGN is a likely candidate to provide Ca^{2+} for sorting at TGN, which could be mediated
126 through an IP3 receptor (IP3R)-dependent mechanism.

127 To investigate if the release of Ca^{2+} from the ER has an impact on the sorting and export
128 of soluble secretory cargo molecules from the TGN, we analyzed trafficking and secretion of the
129 well-established Cab45-clients: cartilage oligomeric protein (COMP) and Lysozyme C (LyzC)
130 (von Blume 2011; von Blume 2012) in the presence and absence of the IP3R antagonist (2-APB)
131 (Maruyama et al., 1997). We used the RUSH (Retention Using Selective Hooks) system to
132 quantify the trafficking and packaging of COMP or LyzC, respectively, into secretory vesicles in
133 HeLa cells in the presence of 2-APB (70 μM) or DMSO (control) (Boncompain et al., 2012). To
134 this end, HeLa cell lines were transfected with RUSH constructs containing COMP-EGFP or
135 LyzC-EGFP to analyze intracellular trafficking of EGFP-fused proteins at different time points
136 after synchronous release from the ER by biotin addition (**Figure 1A**). We observed simultaneous
137 export of COMP-EGFP from the ER in control and 2-APB treated cells (**Figure 1B [0, 20 min]**).
138 However, the appearance of cytosolic vesicles (TGN carriers) was significantly delayed in cells
139 treated with 2-APB compared to control cells at later time points (**Figure 1B, C [30, 40, 60 min]**).

140 To confirm the observed phenotype on a cell population, we performed RUSH experiments
141 using COMP-EGFP as cargo in HeLa cells treated with DMSO (control) or 2-APB with
142 subsequent FACS analysis. We used this assay to quantify the intracellular accumulation of EGFP-
143 COMP in DMSO or 2-APB-treated cells. Cells were fixed at 0, 30, 60, and 120 min after biotin
144 addition, and 10^4 cells for each time point were analyzed by FACS. We calculated the average
145 arithmetical value for the fluorescent intensity of COMP-EGFP obtained from each sample's green
146 emission fluorescence channel. The arithmetical average values for fluorescence intensity of
147 COMP-EGFP from 2-APB treated cells were 1.8 and 2.1-fold higher than in control cells after 60
148 and 120 minutes after biotin addition, respectively, indicating a more extended residence of the
149 EGFP-COMP inside cells in 2-APB treated cells confirming our microscopy observations (**Figure**
150 **1D, Supplementary S1A, S1C**).
151 To correlate these results with the actual TGN exit of the cargo molecules, we applied live-
152 cell imaging of the exiting EGFP-tagged cargo molecules in the presence of the GALNT1-BFP
153 TGN marker. We measured time-dependent changes in fluorescence intensity of EGFP-tagged
154 protein within the ROI of TGN defined by the GALNT1-BFP signal. These results showed that
155 the reduction in the number of vesicles in 2-APB-treated cells in the RUSH experiments was
156 consistent with a prolonged residence of cargo in the TGN compared to DMSO-treated cells
157 (**Figure 1E**). To quantify this phenotype, we applied a non-linear regression function of the
158 intensity values on the plot shown in Figure 1D (**Supplementary S1E**). In addition, we calculated
159 span values for each curve representing changes in LyzC-EGFP intensity within Golgi ROI. The
160 span was defined as the difference between the fluorescence intensity of EGFP at the starting point
161 and the predicted plateau for each curve, representing a change in fluorescence intensity during
162 the experiment. The span value calculated for LyzC-EGFP expressing cells in the presence of 2-

163 APB exhibited a two-fold decrease compared to control cells (span value for 2-APB and DMSO
164 samples were 0.8 and 1.5 respectively), indicating a significant defect in TGN export of LyzC-
165 EGFP in these cells.

166 To further validate that the inhibition of the IP3R reduces the secretion of the Cab45 client
167 LyzC from the cells, we performed a secretion assay. We generated stable cell lines expressing
168 EGFP-tagged LyzC under a constitutive promoter by lentiviral transduction of HeLa cells.
169 Secretion assays were performed in a complete growth medium, and secreted LyzC-EGFP in the
170 supernatant was immunoprecipitated using GFP trap agarose beads before analysis by western
171 blotting. The western blot analysis revealed a 48% reduction in secreted LyzC-EGFP in the 2-
172 APB-treated condition compared to DMSO-treated control cells (**Figure 1F**).

173 These data suggested that the activity of IP3 receptors impacts the TGN export and
174 secretion of Cab45 clients. Previous work has shown that Golgi-localized IP3 receptors have no
175 impact on SPCA1 dependent Ca^{2+} uptake (Wong et al., 2013). Therefore we speculated that Ca^{2+}
176 flow between these organelles might be facilitated by ER-TGN MCS (Ramazanov et al., 2021).

177

178 ***MCS integrity is essential for TGN export of Cab45 clients***

179 VAPA and VAPB proteins are essential in maintaining ER-TGN MCS integrity by
180 tethering ER and TGN. Deleting these proteins from cells reduces contacts between the organelles
181 (Lev, 2010; Phillips and Voeltz, 2016; Venditti et al., 2019b). To examine the role of ER-TGN
182 contact site in the trafficking of Cab45 clients, we performed RUSH experiments and analyzed
183 the trafficking of COMP-EGFP in VAPA/VAPB-depleted HeLa cells. To this end, HeLa cells
184 were transfected with non-targeting siRNA as control or siRNAs targeting VAPA and VAPB.
185 After 24 hours, HeLa cell lines were transfected with RUSH-constructs expressing COMP-EGFP.

186 RUSH experiments were performed, and samples were fixed at different time points after biotin
187 addition. Immunofluorescence images captured at 30, 40, and 60 minutes after biotin addition
188 showed that compared to control cells, VAPA/VAPB siRNA-treated cells exhibited a significant
189 delay in the formation of COMP-EGFP containing post-Golgi vesicles (**Figure 2A [30, 40, 60**
190 **min]**). Consistent with this result, quantification of post-Golgi vesicles at different time points
191 from a randomly selected population of control siRNA or VAPA/VAPB siRNA-treated cells
192 revealed a decrease in the amount of TGN-derived vesicles (**Figure 2B**).

193 We confirmed the delayed export of Cab45 clients seen in VAPA and VAPB knockdown
194 with RUSH LyzC or COMP, respectively, in control versus VAPA/VAPB-dKO HeLa cell lines
195 (Dong et al., 2016) (see immunofluorescence **Supplementary S2A, S2B [0, 20 min]**), and
196 quantification (**Supplementary S2C, S2D**). In parallel, we measured the time-dependent
197 intracellular decrease of COMP-EGFP by FACS in control versus VAPA/VAPB deficient cells.
198 The average intensity values in the GFP channel from VAPA and VAPB deficient cells were 1.5-
199 fold higher than in control cells at 60 and 120 minutes after biotin addition, indicating
200 accumulation of COMP-EGFP in these cells (**Figure 2C, Supplementary S1A, S1C**).

201 To demonstrate that the secretion defect is caused by impaired TGN export, we performed
202 live-cell imaging of the exiting EGFP-tagged Cab45 clients in the presence of the GALNT1-BFP
203 TGN marker. We observed time-dependent changes in LyzC-EGFP intensity within the TGN ROI
204 and a 1.6-fold difference in span values in control versus VAPA and VAPB-depleted cells. In
205 addition, we observed a prolonged residence of LyzC in the TGN of HeLa cell lines transfected
206 with siRNA to VAPA and VAPB compared to control cells (**Figure 2D, Supplementary S1F**).
207 The efficiency of knockdowns of VAPA and VAPB proteins was analyzed by western blotting
208 (**Figure 2E**).

209 To investigate whether this phenotype is specific for certain soluble secretory proteins and
210 does not affect other proteins transported by bulk flow secretion, we measured the time-dependent
211 intracellular decrease of COMP-EGFP and EQ-sol-GFP by FACS in control versus VAPA/VAPB
212 deficient HeLa cells as well as 2-APB treated cells. These data indicated that the secretion of EQ-
213 sol-GFP, a non-specific marker of bulk flow secretion (Deng et al., 2016), is unaffected by VAPA
214 and VAPB-depletion (**Suppl. S1A-C**).

215 Together these data showed that the TGN export of the Cab45 clients COMP and LyzC
216 from TGN requires intact MCSs between ER and TGN (**Figure 2**) and IP3R-dependent Ca^{2+}
217 release from the ER (**Figure 1**). These data also suggest that ER-TGN MCS could serve as
218 potential sites for Ca^{2+} transfer.

219

220 ***Targeting Twitch-based FRET sensors to ER-TGN MCS***

221 Our next goal was to test potential Ca2+ flow at ER-TGN MCSs directly. These MCSs
222 would be potential structures that could serve as hotspots for Ca^{2+} transfer between the organelles.
223 To evaluate possible Ca^{2+} flows in these sites, we used Förster resonance energy transfer (FRET)-
224 based Ca^{2+} biosensors called Twitch. These sensors contain a minimal Ca^{2+} binding moiety derived
225 from the C-terminal domain of troponin C incorporated between mCerulean3 and cpVenuscd
226 (Thestrup et al., 2014). To target the sensors to ER-TGN MCS in living cells, we introduced an
227 amino acid sequence coding the N-terminal region of OSBP1, including a PH domain and an FFAT
228 motif (**Figure 3A**). As the N-terminal disordered domain of OSBP seems to be crucial for active
229 lipid transport in the ER-TGN MCS (Jamecna et al., 2019), we generated sensors containing a
230 disordered domain (N-PH-FFAT) as well as a sensor without that domain (PH-FFAT)
231 (**Supplementary S3A, S3B**). We constructed stable HeLa cell lines expressing the MCS-Twitch

232 sensors under a doxycycline-inducible promoter to obtain stable and equal protein expression
233 levels. We confirmed the expression of the respective sensor after doxycycline induction by
234 immunofluorescence and live-cell imaging (**Supplementary S3B**). To investigate the correct
235 localization of the sensors at the TGN, cells were fixed and stained with antibodies recognizing
236 GM130 or TGN46. Immunofluorescence microscopy data confirmed that the MCS-Twitch sensors
237 expressed in HeLa cells correctly localize (**Supplementary S3C, S3D**).
238
239 ***The Twitch2b-MCS FRET sensor detects Ca^{2+} flows***
240 To determine the range of Ca^{2+} signals detectable at the MCS at steady-state (non-treated
241 cells incubated at 37°C), we constructed four MCS-Twitch sensors with different Ca^{2+} affinities
242 (depicted in **Supplementary Tables 1, 2**). For quantitative FRET measurements of Ca^{2+}, we
243 calculated the FRET index value in the cell line expressing the respective sensor as an
244 approximation of the FRET/molecule (Grashoff et al., 2010; Kumar et al., 2016). The normalized
245 FRET index values were acquired by measuring FRET intensity, subtracting the background noise
246 and the bleed-through for the two fluorophores, and normalizing them to FRET acceptor intensity.
247 Measuring FRET indexes from the MCS-Twitch sensors at steady revealed that compared to MCS-
248 Twitch9x, MCS-Twitch7x, and MCS-Twitch8x, the Twitch2b sensor showed the highest FRET
249 index (**Supplementary S3E**).
250 We performed a series of control experiments to test if the Twitch2b sensor was responsive
251 to Ca2+ perturbations in the cells. First, we determined the FRET values in HeLa cells expressing
252 the respective MCS-Twitch sensor by live-cell fluorescence microscopy in cells treated with
253 DMSO (control) or the Ca^{2+} chelating agent BAPTA-AM. As expected, chelating intracellular
254 Ca^{2+} ions with BAPTA-AM significantly decreased the FRET index of MCS-Twitch2b (**Figure**

255 **3E, F**). However, the FRET indices of MCS-Twitch2b upon treating the cells with BAPTA were
256 similar to the baseline levels of the low Ca^{2+} affinity MCS-Twitch7x, 8x and 9x sensors (**Figure**
257 **C, D; Supplementary S3E**). Therefore, Twitch2b was selected for all further experiments.

258 To quantify the range of free Ca^{2+} concentrations, we calibrated the Twitch2b sensor. To
259 calibrate Twitch2b in live cells, we used HeLa cells stably expressing CYTO-Twitch2b. We
260 applied a reciprocal dilution of buffers containing increasing ratios of Ca-EGTA/K2-EGTA
261 concentrations, and the free Ca^{2+} ion concentrations were calculated as described in Materials and
262 Methods (**Supplementary S4A, S4B**). The FRET indexes obtained from Twitch2b at different
263 ratios of Ca-EGTA/K2-EGTA in the calibration experiment allowed us to build a calibration curve
264 that demonstrated a strong correlation between the FRET index value and the concentration of free
265 Ca^{2+} (calibration plot shown in **Figure 3B**). Thus, we developed a powerful tool to measure Ca^{2+}
266 levels in the ER-TGN-MCS. We developed a tool that accurately measures Ca2+ levels in the ER-
267 TGN-MCS.

268 To measure the effects of increased intracellular Ca^{2+} concentrations on the FRET signals
269 from MCS-Twitch2b sensors, we utilized active and passive means of increasing cytosolic Ca^{2+}
270 levels. Treatment of cells with ionomycin, which raises the intracellular Ca^{2+} level, significantly
271 increased the FRET index (Figure 3G, H). Several signaling pathways, including cell surface
272 receptors, are known to utilize Ca^{2+} ions as second messengers for the downstream signaling
273 (Carafoli, 2002; Dickenson and Hill, 1994; Thillaiappan et al., 2017). Activation of Histamine
274 receptors (H1-receptor) at the plasma membrane causes the activation of PLC, which in turn
275 elevates intracellular Ca^{2+} through an IP3-dependent mechanism. To test if the MCS sensor detects
276 these signals, we performed the FRET measurements in HeLa cells expressing PH-FFAT-
277 Twitch2b incubated with either DMSO (control) or after treatment with histamine. (**Figure 3I, J**).

278 The data showed an increase in the FRET index– revealing a physiological link between MCS
279 Ca^{2+} levels and the signaling receptor IP3.
280 Because we did not observe differences in the FRET index between PH-FFAT-Twitch and
281 N-PH-FFAT-Twitch sensors (**Supplementary 3E, 3F, 3G, 3H**), we decided to perform further
282 experiments using the PH-FFAT targeting motif.
283 The data indicates that the release of Ca^{2+} caused by IP3R stimulation leads to an increase
284 in Ca^{2+} levels in MCS and that our sensor sensitively detects these changes.
285
286 ***TGN protein abundance and Ca^{2+}flux at MCS are coupled***
287 Our previous work showed that TGN Ca^{2+} influx is necessary for the TGN exit of secretory
288 proteins (Crevenna et al., 2016; Deng et al., 2018; Kienzle et al., 2014; von Blume et al., 2011).
289 Therefore, we hypothesized that there must be a correlation between cargo influx into the TGN
290 and Ca^{2+} flow in the MCS. To test if Ca^{2+} in ER-TGN MCSs is influenced by protein abundance,
291 we treated HeLa cells expressing MCS-Twitch 2b with Cycloheximide (CHX) to block *de novo*
292 protein synthesis. We incubated cells for 1, 2, and 4 hours and analyzed FRET signals. We
293 observed a time-dependent decrease in the FRET index of cells treated with CHX. To further
294 demonstrate that this is correlated with cargo abundance in the TGN, we incubated HeLa cells
295 expressing MCS-Twitch 2b at 20°C to arrest secretory proteins in the TGN (Ladinsky et al., 2002;
296 Matlin and Simons, 1983). Notably, FRET values were significantly decreased in cells incubated
297 at 20°C (**Figure 4A, B**). However, duration of the 20°C block for more than 1 hour did not affect
298 the average FRET index values (**Figure 4C**). More importantly, incubation of cells at 37°C after
299 the 20°C-block resulted in a complete recovery of the FRET index (**Figure 4B, C)**. To validate
300 that the changes in the FRET indices were not due to other factors, cells were incubated at 37°C

301 and 20°C in the presence of ionomycin (**Figure 4E**). Independent of the incubation temperature,
302 ionomycin treatment led to a recovery of FRET indexes, demonstrating that the effects are specific
303 to Ca^{2+}. These data supported that the presence of newly synthesized protein stimulates the Ca2+
304 flux in the MCS. Furthermore, we showed that this is specific to the cargo abundance in the TGN.

305 In the current study, we quantify the abundance of Ca^{2+} flux in the ER-TGN MCS, which
306 has remained unknown. We also demonstrate that cargo entering the TGN elicits a Ca^{2+} release in
307 the MCS required for sorting Cab45 clients into a TGN-derived carrier (**Figure 5A**).

308 Our previous work showed that SPCA1, the only Ca^{2+} ATPase in the TGN, is required for
309 secretory cargo sorting in the TGN (von Blume et al., 2011). Interestingly, these studies also
310 exemplified that the Ca^{2+} binding protein Cab45 oligomerizes and forms a scaffold for collecting
311 its clients, including LyzC and COMP (Crevenna et al., 2016; von Blume et al., 2012).
312 Furthermore, sphingomyelin produced by SMS1 promotes SPCA activity and Cab45/client export
313 from the TGN (Deng et al., 2018). However, the source of Ca^{2+} that drives the process has
314 remained unknown (Ramazanov et al., 2021). In the current work, we demonstrate that the TGN
315 export of COMP and LyzC requires the integrity of the ER-TGN MCS and IP3R-dependent Ca^{2+}
316 fluxes in the MCS, suggesting that Ca^{2+} transfer between these organelles is the primary source
317 for SPCA1.

318 The autoregulation of the secretory pathway by cellular signaling remains mysterious.
319 However, central principles have been uncovered in recent years (Di Martino et al., 2019). On the
320 other hand, the signaling pathway that stimulates the Ca^{2+} release through the contact site remains
321 unknown. Our work shows that it is directly linked to IP3 production and activation of IP3R close
322 to ER-TGN contact sites. Although current work provides an understanding of upstream signaling
323 events that regulate of sorting of soluble proteins at TGN and depend on the activity of SPCA1,

324 the possibility that LyzC and COMP themselves could serve as a stimulus for the activation of

325 such pathways remains to be investigated.

326 ## Materials and Methods

327 **DNA techniques and plasmid construction**

328 Restriction enzymes for molecular biology were obtained from New England Biolabs.
329 PCRs were performed with a Phusion Polymerase (Thermofisher) and a Mastercycler Nexus
330 (Eppendorf). All plasmids used in this study bear ampicillin resistance for selection in *Escherichia*
331 *coli* and are listed in Table 1, where the transgenes and inserts are described. The DNA sequences
332 encoding PH-FFAT/N-PH-FFAT domains of OSBP1 fused with Twitch sensors were integrated
333 into the donor plasmid of the transposon-based piggyBac system for stable transgene-expressing
334 cell lines generation (Li et al., 2013). The piggyBac backbone vector (PB-T-PAF) and PB-RN and
335 PBase were a gift from James Rini, University of Toronto, Ontario, Canada (Li et al., 2013). In
336 brief, to generate PB-T-PAF-PHFFAT-Twitch constructs, the PB-T-PAF vector was linearized
337 with NheI and NotI-HF restriction enzymes (NEB). PH-FFAT/N-PH-FFAT sequences (5'-
338 NheI/3'-AscI) were amplified by PCR from pLJM1-FLAG-GFP-OSBP plasmid
339 (Addgene#134659). The sequences encoding Twitch (Twitch2b/Twitch7x/Twitch8x/Twitch9x)
340 Calcium sensors were obtained from plasmids that have been generously provided by Oliver
341 Griesbeck Lab and were amplified by adding corresponding restriction sites (5'-AscI/3'-NotI). All
342 fragments were ligated in the PB-T-PAF backbone. All cloning experiments were conducted using
343 Phusion High-Fidelity Polymerase and T4 ligase (Thermo Fisher Scientific) according to the
344 manufacturer's instructions. Similar strategies generated VAPA-Twitch2b and CYTO-Twitch2b
345 constructs. The sequences encoding Twitch2b for these constructs were amplified by adding
346 corresponding restriction sites (5'-NheI/3'-AscI). The VAPA fragment was amplified from
347 plasmid coding full-length VAPA protein and was gifted from Pietro De Camilli with addition of
348 AscI and NotI restriction sites. CYTO-Twitch2b construct was generated from VAPA-Twitch2b

349 by replacing the VAPA sequence with short stop-codon containing fragment, annealed by using
350 the following sequences (5'CGCGCCAGAGGAGTTTTAAGC3' and
351 5'GGCCGCTTAAAACTCCTCTGG3'). pLenti-LyzC-EGFP for secretion assay lines was
352 generated using gateway cloning reaction by amplifying LyzC-EGFP from plpcx-LyzC-EGFP and
353 cloning into pDONR221 using BP cloning reaction and then subsequently using LR cloning
354 reaction into the destination vector to generate the desired construct. The correct sequence of all
355 constructs was confirmed by DNA sequencing using the SmartSeq Kit from Eurofins Genomics
356 or KECK sequencing (Yale University).

357 **Cell culture and generation of stable cell lines expressing Calcium sensor constructs.**

358 Cell lines were maintained in DMEM media (Gibco) containing 10% FBS (Sigma
359 12306C-500ML) at 37°C and 5% CO_2. For transfection, cells were plated in antibiotic-free media
360 24 hours before the procedure. DNA transfections were performed using Lipofectamine 2000
361 reagent according to the manufacturer's protocol. After 8 hours, the media was replaced.
362 Transgene expression was estimated at 48 hours after transfection. To generate cell lines stably
363 expressing the mentioned transgenes HeLa lines were used. In brief, HeLa cells at 70% confluency
364 were transfected with PB-T-PAF (with the corresponding transgene), PB-RN, and PBase (total
365 DNA 1.5 µg; at ratio 8:1:1) using Lipofectamine 2000 in OptiMEM-I media. Cells were selected
366 for 48 hours with 2 µg/ml puromycin dihydrochloride (Sigma-Aldrich) and for 7 days with 400
367 µg/ml G418 disulfate salt (A1720-5G, Sigma-Aldrich). To induce transgene expression, cells were
368 incubated in the presence of doxycycline (J63805 Alfa Aesar, USA) (1ug/mL) for 24 hours. The
369 generated lines were sorted on BD FACS Aria to exclude resistant cells without transgene
370 expression.

371 HeLa cell lines stably expressing LyzC-EGFP were generated using lentiviral transduction
372 containing pLenti-LyzC-EGFP construct with followed Blasticidin 8 ug/mL (InvivoGen)
373 selection for 48 hours. siRNA transfections were performed using Lipofectamine RNAiMAX
374 according to standard protocol. VAPA/VAPB-dKO lines were generated by Pietro De Camilli Lab
375 and published previously (Dong et al., 2016).

376 **RUSH cargo sorting assay and fluorescent microscopy**

377 RUSH assays were performed as described previously (Boncompain et al., 2012; Deng et
378 al., 2018). Studied cell lines were cultured in 6-well plates (Cat#353046, Corning) on glass slides
379 (Cat. #72290-04, EMS) and transfected with RUSH-COMP-EGFP and RUSH-LyzC-EGFP
380 constructs using Lipofectamine 2000 according to standard protocol. At 24 hours post-transfection,
381 cells were incubated with 40 µM d-Biotin (Sigma) ingrown media for different time points (20,
382 30, 40, 60, and 90 min or without d-Biotin (control). For IF slides, cells were washed once with
383 PBS, fixed in 4% PFA (Electron Microscopy Sciences) in PBS for 10 min, and mounted on 12mm
384 coverslips (Electron Microscopy Sciences) using ProLong Gold (Thermo Fisher Scientific).
385 Nuclear chromatin was stained by short incubation in 2.5uM DAPI (Biolegend) solution.
386 Acquisition of EGFP was performed using a Delta Vision system by imaging z-stacks with a step
387 size of 0.2 µm.

388 We empirically measured the sizes of objects between 4 and 20 pixels for quantification of
389 vesicles using the Analyze Particles function in ImageJ, which detects vesicular carriers but omits
390 larger objects such as the Golgi. While small-fragmented and isolated Golgi structures could be
391 detected in error. Furthermore, only vesicles of cells expressing the RUSH construct were counted.
392 The Fiji macro count_fixed_vesicles_V1.3 (M. Pakdel), including the Particle Analyzer plug-in

393 by Fiji, was used to determine the number of vesicles (Deng et al., 2018). Kruskal–Wallis one-
394 way analysis of variance was used for comparisons in RUSH experiments.

395 Cells were cultured in six wells on glass slides for immunostaining and fixed for 10 min
396 with 4% paraformaldehyde. After washing with PBS, cells were permeabilized for 5 min in 0.2%
397 Triton-X 100 and 0.5% SDS in 4% BSA. After washing with PBS, cells permeabilized with Triton-
398 X 100 were blocked with 4% BSA for 1 h. Next, cells were incubated with primary followed by
399 the corresponding secondary antibody for 1 h at room temperature in a blocking buffer in the dark.
400 Slides were washed three times with PBS after incubation with antibody. Glass slides were
401 mounted with ProLong Gold (Thermo Fisher Scientific). Antibodies to TGN46 (AHP500G,
402 Biorad) and GM130 (610822, BD) were used at dilution 1:200.

403 For FACS analysis cells were fixed with 4% PFA for 10 min. After fixation washed with
404 ice-cold DPBS and dissociated using trypsin-EDTA solution. Cells were washed with DPRS three
405 times by centrifugation at 200g for 5 min each. FACS analysis was performed using BD LSRII
406 machine. 10000 cells were analyzed for each sample. FACS data were analyzed using FlowJo
407 10.5.3 for Windows.

408

409 **RUSH protein trafficking analysis**

410 HeLa cells were seeded on Mattek dishes (p35gc-1.5-14-c, Mattek) and cultured at 37°C
411 with 5% CO_2. The next day or the day before imaging, cells were transfected by Lipofectamine
412 2000 (Invitrogen) with two plasmids expressing GalT-BFP (a trans-Golgi maker from James
413 Rothman lab) and RUSH COMP or RUSH Lysozyme C (see above for details of the plasmids).
414 After five to eight hours, cells were washed and incubated with DMEM with 10% FBS overnight.
415 Before imaging, cells were washed and briefly incubated with 37°C-warmed DMEM

416 supplemented with 10% FBS and HEPES buffer (Gibco, 21063029). Cells were then staged on the
417 microscope as described below.

418 Live-cell imaging was performed using a spinning disk confocal microscope CSUXfw-
419 06p-01 (Yokogawa) on a Nikon eclipse Ti2 (LWD NA=0.52) microscope stand with a motorized
420 stage with stage top Piezo. sCMOS camera Photometrics Prim 95B and CFI Plan Apo Lambda
421 60x oil objective were used. Also, the Oko Lab temperature control system was set to 37°C, and
422 the fluorescence (405 nm and 488 nm) was induced using an Agilent laser combiner. Images were
423 acquired using Nikon Elements. Fluorescence images were taken every three minutes after adding
424 biotin (see above for the methods for RUSH experiments). At each time point, the Nikon Elements
425 stitched 6x5 fields to generate relatively large field images that could accommodate at least 10
426 distinguished secretion events through 90 or 120 minutes.

427 The time-course images generated above were imported to Fiji (ImageJ). Images
428 containing individual cells with distinguishable Golgi and RUSH signals were cropped and stored
429 separately. The Golgi masks were generated using GalT-BFP signals (405 nm excitation) and
430 ImageJ Auto-threshold and imported as ROIs. The Golgi ROIs were used to measure mean RUSH
431 intensity in the Golgi at each time point. The mean RUSH intensities were subtracted from the
432 background signals. Then, the maximum mean value of RUSH during the time course of the single-
433 cell images was used to divide the RUSH intensities, thus normalizing the maximal RUSH
434 intensities in the Golgi marker set to 1. The time course images for every cell were analyzed
435 separately and combined to generate the mean RUSH intensity in each time point and its standard
436 deviation, as described in the Figures. Three independently cultured cells were analyzed, and their
437 images were combined to generate the final data.

438 **Secretion assay of LyzC-EGFP**

439 For the secretion assay, $5x10^5$ cells stably expressing LyzC-EGFP were plated in a 6-well
440 plate. After 24 hours, cells were pretreated with 70μM 2-APB and DMSO. After that incubated in
441 a grown medium containing 2-APB and DMSO for 1 hour. Cells and media were collected
442 separately. Cells were lysed using RIPA buffer. Collected growth media was incubated overnight
443 with GFP-trap beads at 4°C. The following day the beads were washed 4 times with DPBS, and
444 then protein was eluted from the beads by boiling it in 2X Laemmli SDS sample buffer (Biorad).
445 Cell lysates and IP fractions were analyzed by western blotting.

446 **Live cell imaging and FRET analysis.**

447 For live cell imaging, DMEM without phenol red containing 4.5 mg ml – glucose, 25 mM
448 HEPES, and 2 mM glutamine (Life Technologies) supplemented with 10 % FBS was used. Cells
449 were seeded on Glass bottom dishes (D35-14-1.5-N, Cellvis) at a density $5x10^4$ per dish. The next
450 day to induce transgene expression, doxycycline at a final concentration of 1ug/mL was added.
451 After 24 hours, doxycycline was removed, and cells were incubated in imaging media for an
452 additional 24 hours. ImageJ (National Institutes of Health) was used for basic image processing.
453 All analyses were done using custom-written software (MATLAB R2014a; MathWorks). To
454 manipulate intracellular Ca^{2+} levels as well as induce Ca^{2+} flux following drugs at corresponding
455 concentrations were used: calcium ionomycin (I3909-1ML, Sigma) at 1μM; 2-APB (100065-
456 100MG, Millipore) at 70μM, Histamine (H7125-1G, Sigma) 1 μM solution, BAPTA-AM
457 (126150-97-8, Millipore) at 25 μM final concentration. Cells were treated with cycloheximide to
458 inhibit protein synthesis at a concentration of 10ug/mL (DSC81040-5, Dot Scientific Inc).

459 **FRET sensor calibration experiment.**

460 Free Ca^{2+} calibration solutions were made using Calcium Calibration Buffer Kit #1 (Cat.
461 No. C3008MP, Biotium) according to standard protocol. To perform the FRET calibration

462 experiment, the HeLa cell line stably expressing CYTO-Twitch2b was used. $1x10^5$ cells were
463 plated into Glass bottom dishes (D35-14-1.5-N, Cellvis), and doxycycline was added to the media
464 at a final concentration of 1 ug/mL. After 24 hours, each plate was washed twice with 10mM
465 EGTA, 100mM KCl, and 10mM MOPS (pH 7.2). To chelate residual Ca^{2+}, cells were incubated
466 in 10mM EGTA, 100mM KCl, and 10mM MOPS (pH 7.2) with 1 μM ionomycin for 20 min at
467 RT. 2ml of stock solutions with free Ca^{2+} concentrations ranging from 0 μM to 39 μ μM were
468 added to cells, and FRET indexes were measured for each condition

469 **FRET imaging and analysis**

470 These analyses were done as previously described by (Kumar et al., 2016). High-resolution
471 live FRET imaging was performed on Nikon Eclipse Ti widefield microscope equipped with a
472 cooled charged-coupled device Cool SNAP HQ2 camera, using a ×100, 1.49 NA oil objective at
473 37 °C. Images were acquired using Micromanager software. Three sequential images with 500 ms
474 exposure time were acquired with the following filter combinations: donor (Teal) channel with
475 460/20 (excitation filter-ex), T455lp (dichroic mirror-di), and 500/22 (emission filter-em); FRET
476 channel with 460/20 (ex), T455lp (di) and 535/30 (em); and acceptor (Venus) channel with 492/18
477 (ex), T515lp (di) and 535/30 (em) filter combinations. All filters and dichroic were purchased from
478 Chroma Technology. For data analysis, donor leakage was determined from HeLa cells transiently
479 transfected with Vinculin-Teal, whereas acceptor cross excitation was obtained from Vinculin-
480 Venus transfected cells. For all the calculations, respective background subtraction, illumination
481 gradient, and pixel shift correction were performed, followed by three-point smoothening. The
482 slope of the pixel-wise donor or acceptor channel intensity versus FRET channel intensity gives
483 leakage (x) or cross-excitation (y) fractions, respectively. FRET map and pixel-wise FRET index

484 for the sensors were determined from FRETindex = [FRETchannel−x(Donorchannel)−
485 y(Acceptorchannel)]/[Acceptorchannel]

486 ImageJ (National Institutes of Health) was used for basic image thresholding. Mean FRET
487 index per cell was calculated for each region within the mask. Then, a student t-test was performed
488 between the two groups to calculate statistical significance and p-value. At least $P < 0.05$ was
489 considered significant. All analyses were done using custom-written software (MATLABR2020b;
490 MathWorks) (Kumar et al., 2016).

491 **siRNA delivery and western blotting**

492 Knockdown of VAPA and VAPB proteins was performed using siRNA (VAPA: 5'-
493 AACTAATGGAAGAGTGTAAAA-3'; VAPB: 5'-AAGAAGGTTATGGAAGAATGT-
494 3')(Wakana et al., 2021). Non-targeting siRNA was purchased from Qiagen (Catalog No. –
495 1027281) and used as a negative reference control. The knockdown of VAPA and VAPB proteins
496 was achieved by combined transfection (siVAPA and siVAPB) using LipofectRNAiMAX
497 according to standard protocol. Knockdown efficiency was confirmed by Western blotting of cell
498 lysates in radioimmunoprecipitation assay (RIPA) buffer (50 mM Tris-HCl, pH 7.4 [American
499 Bioanalytical], 150 mM NaCl [American Bioanalytical], 1% Triton X100 [American
500 Bioanalytical], 1% sodium deoxycholate [Sigma-Aldrich], and 0.1% SDS [American
501 Bioanalytical] in Milli-Q water); protease and phosphatase inhibitor (Thermo Fisher Scientific)
502 was added just before extraction. The cell lysate was resolved using SDS-PAGE and transferred
503 to the nitrocellulose membrane (Biorad Laboratories) using a transfer system (Trans-Blot Turbo;
504 Bio-Rad Laboratories). The membrane was blocked using 5% skimmed milk (American
505 Bioanalytical) in TBS with 0.1% Tween 20 (TBST) for 1 hour and incubated with the following
506 primary antibodies diluted in 5% milk with TBST overnight at 4°C: Anti-β-actin (1:5000, A5441-

507 .2ML Sigma); Anti-VAPA (1:1000, SAB1402460-100G, Sigma); Anti-hVAPB (1:2000,
508 MAB58551 R&D systems); anti-GFP (1:1000, 11814460001, Roche). The membrane was washed
509 3 times with 5% milk TBST and incubated with HRP-conjugated secondary antibodies (1:5000,
510 32230/32260; Invitrogen). Data were visualized using chemiluminescence detection on ChemiDoc
511 Touch (Bio-Rad Laboratories)**.**

512 **Graphical data and image design**

513 Graphs were plotted in GraphPad Prism version 9.2.0 for Mac, GraphPad Software, San Diego,
514 California, USA. Images were compiled using Adobe Illustrator 2022 (Adobe Inc. (2022). Adobe
515 Illustrator. Retrieved from https://adobe.com/products/illustrator). Schemes were designed using
516 Biorender software (biorender.com).

517

518

Acknowledgments

We thank Dr. Pietro de Camilli for providing VAPA/VAPB-dKO cell lines and the Burd lab for discussions and support. Julia von Blume is funded by a Yale-start grant and by the National Institute of General Medical Sciences of the NIH under the award number GM134083-01, an Administrative Supplement 3R01GM134083-03S1 and a Project and Feasibility award from Yale Diabetic Research Center (GR112420).

Author Contributions

B. R. Ramazanov and J. von Blume designed the experiments. B. R. Ramazanov carried out the experiments and analyzed the data. A. Kumar and M. Schwartz supported FRET data analysis and composed the software code for data analysis. A. Parchure, and Y. Kim performed and analyzed secretion assays. O. Griesbeck provided Twitch sensors encoding plasmids. M. Schwartz provided the equipment. B. R. Ramazanov and J. von Blume wrote the paper.

Declaration of Interest

The authors declare no competing financial interests.

534 **Abbreviations**

535 ER - Endoplasmic reticulum

536 FRET - Fluorescence resonance energy transfer

537 nm - nanometer

538 TGN - Trans Golgi Network

539

540 **References**

541 Barlowe, C.K., and E.A. Miller. 2013. Secretory protein biogenesis and traffic in the early
542 secretory pathway. *Genetics*. 193:383-410.
543 Berridge, M.J., M.D. Bootman, and H.L. Roderick. 2003. Calcium signalling: dynamics,
544 homeostasis and remodelling. *Nat Rev Mol Cell Biol*. 4:517-529.
545 Boncompain, G., S. Divoux, N. Gareil, H. de Forges, A. Lescure, L. Latreche, V. Mercanti, F.
546 Jollivet, G. Raposo, and F. Perez. 2012. Synchronization of secretory protein traffic in
547 populations of cells. *Nat Methods*. 9:493-U120.
548 Carafoli, E. 2002. Calcium signaling: A tale for all seasons. *Proceedings of the National*
549 *Academy of Sciences*. 99:1115-1122.
550 Crevenna, A.H., B. Blank, A. Maiser, D. Emin, J. Prescher, G. Beck, C. Kienzle, K. Bartnik, B.
551 Habermann, M. Pakdel, H. Leonhardt, D.C. Lamb, and J. von Blume. 2016. Secretory
552 cargo sorting by Ca2+-dependent Cab45 oligomerization at the trans-Golgi network. *J*
553 *Cell Biol*. 213:305-314.
554 De Matteis, M.A., and A. Luini. 2008. Exiting the Golgi complex. *Nat Rev Mol Cell Biol*. 9:273-
555 284.
556 Deng, Y., M. Pakdel, B. Blank, E.L. Sundberg, C.G. Burd, and J. von Blume. 2018. Activity of
557 the SPCA1 Calcium Pump Couples Sphingomyelin Synthesis to Sorting of Secretory
558 Proteins in the Trans-Golgi Network. *Dev Cell*. 47:464-478 e468.
559 Deng, Y., F.E. Rivera-Molina, D.K. Toomre, and C.G. Burd. 2016. Sphingomyelin is sorted at
560 the trans Golgi network into a distinct class of secretory vesicle. *Proc Natl Acad Sci U S*
561 *A*. 113:6677-6682.
562 Di Martino, R., L. Sticco, and A. Luini. 2019. Regulation of cargo export and sorting at the
563 trans-Golgi network. *FEBS Lett*. 593:2306-2318.
564 Dickenson, J.M., and S.J. Hill. 1994. Selective potentiation of histamine H1-receptor stimulated
565 calcium responses by 1,4-dithiothreitol in DDT1MF-2 cells. *Biochem Pharmacol*.
566 48:1721-1728.
567 Dong, R., Y. Saheki, S. Swarup, L. Lucast, J.W. Harper, and P. De Camilli. 2016. Endosome-ER
568 Contacts Control Actin Nucleation and Retromer Function through VAP-Dependent
569 Regulation of PI4P. *Cell*. 166:408-423.
570 Gillon, A.D., C.F. Latham, and E.A. Miller. 2012. Vesicle-mediated ER export of proteins and
571 lipids. *Biochim Biophys Acta*. 1821:1040-1049.
572 Grashoff, C., B.D. Hoffman, M.D. Brenner, R. Zhou, M. Parsons, M.T. Yang, M.A. McLean,
573 S.G. Sligar, C.S. Chen, T. Ha, and M.A. Schwartz. 2010. Measuring mechanical tension
574 across vinculin reveals regulation of focal adhesion dynamics. *Nature*. 466:263-266.
575 Guo, Y.S., D.W. Sirkis, and R. Schekman. 2014. Protein Sorting at the trans-Golgi Network.
576 *Annu Rev Cell Dev Bi*. 30:169-206.
577 Kawano, M., K. Kumagai, M. Nishijima, and K. Hanada. 2006. Efficient trafficking of ceramide
578 from the endoplasmic reticulum to the Golgi apparatus requires a VAMP-associated
579 protein-interacting FFAT motif of CERT. *J Biol Chem*. 281:30279-30288.
580 Kelly, R.B. 1985. Pathways of Protein Secretion in Eukaryotes. *Science*. 230:25-32.
581 Kienzle, C., N. Basnet, A.H. Crevenna, G. Beck, B. Habermann, N. Mizuno, and J. von Blume.
582 2014. Cofilin recruits F-actin to SPCA1 and promotes Ca2+-mediated secretory cargo
583 sorting. *J Cell Biol*. 206:635-654.

584 Kienzle, C., and J. von Blume. 2014. Secretory cargo sorting at the trans-Golgi network. *Trends*
585 *Cell Biol*. 24:584-593.
586 Kumagai, K., and K. Hanada. 2019. Structure, functions and regulation of CERT, a lipid-transfer
587 protein for the delivery of ceramide at the ER-Golgi membrane contact sites. *Febs*
588 *Letters*. 593:2366-2377.
589 Kumar, A., M. Ouyang, K. Van den Dries, E.J. McGhee, K. Tanaka, M.D. Anderson, A.
590 Groisman, B.T. Goult, K.I. Anderson, and M.A. Schwartz. 2016. Talin tension sensor
591 reveals novel features of focal adhesion force transmission and mechanosensitivity. *J Cell*
592 *Biol*. 213:371-383.
593 Ladinsky, M.S., C.C. Wu, S. McIntosh, J.R. McIntosh, and K.E. Howell. 2002. Structure of the
594 Golgi and distribution of reporter molecules at 20 degrees C reveals the complexity of the
595 exit compartments. *Mol Biol Cell*. 13:2810-2825.
596 Lebreton, S., S. Paladino, D. Liu, M. Nitti, J. von Blume, P. Pinton, and C. Zurzolo. 2021.
597 Calcium levels in the Golgi complex regulate clustering and apical sorting of GPI-APs in
598 polarized epithelial cells. *Proc Natl Acad Sci U S A*. 118.
599 Lehto, M., and V.M. Olkkonen. 2003. The OSBP-related proteins: a novel protein family
600 involved in vesicle transport, cellular lipid metabolism, and cell signalling. *Biochim*
601 *Biophys Acta*. 1631:1-11.
602 Lev, S. 2010. Non-vesicular lipid transport by lipid-transfer proteins and beyond. *Nat Rev Mol*
603 *Cell Biol*. 11:739-750.
604 Li, Z.J., I.P. Michael, D.X. Zhou, A. Nagy, and J.M. Rini. 2013. Simple piggyBac transposon-
605 based mammalian cell expression system for inducible protein production. *P Natl Acad*
606 *Sci USA*. 110:5004-5009.
607 Lissandron, V., P. Podini, P. Pizzo, and T. Pozzan. 2010. Unique characteristics of Ca2+
608 homeostasis of the trans-Golgi compartment. *Proc Natl Acad Sci U S A*. 107:9198-9203.
609 Maruyama, T., T. Kanaji, S. Nakade, T. Kanno, and K. Mikoshiba. 1997. 2APB, 2-
610 aminoethoxydiphenyl borate, a membrane-penetrable modulator of Ins(1,4,5)P3-induced
611 Ca2+ release. *J Biochem*. 122:498-505.
612 Masone, M.C., V. Morra, and R. Venditti. 2019. Illuminating the membrane contact sites
613 between the endoplasmic reticulum and the trans-Golgi network. *FEBS Lett*. 593:3135-
614 3148.
615 Matlin, K.S., and K. Simons. 1983. Reduced temperature prevents transfer of a membrane
616 glycoprotein to the cell surface but does not prevent terminal glycosylation. *Cell*. 34:233-
617 243.
618 Mesmin, B., J. Bigay, J. Polidori, D. Jamecna, S. Lacas-Gervais, and B. Antonny. 2017. Sterol
619 transfer, PI4P consumption, and control of membrane lipid order by endogenous OSBP.
620 *Embo J*. 36:3156-3174.
621 Mesmin, B., J. Bigay, J.M. von Filseck, S. Lacas-Gervais, G. Drin, and B. Antonny. 2013. A
622 Four-Step Cycle Driven by PI(4)P Hydrolysis Directs Sterol/PI(4)P Exchange by the ER-
623 Golgi Tether OSBP. *Cell*. 155:830-843.
624 Missiaen, L., L. Dode, J. Vanoevelen, L. Raeymaekers, and F. Wuytack. 2007. Calcium in the
625 Golgi apparatus. *Cell Calcium*. 41:405-416.
626 Mostov, K.E., and M.H. Cardone. 1995. Regulation of protein traffic in polarized epithelial cells.
627 *Bioessays*. 17:129-138.
628 Pakdel, M., and J. von Blume. 2018. Exploring new routes for secretory protein export from the
629 trans-Golgi network. *Mol Biol Cell*. 29:235-240.

630 Pfeffer, S.R., and J.E. Rothman. 1987. Biosynthetic protein transport and sorting by the
631 endoplasmic reticulum and Golgi. *Annu Rev Biochem*. 56:829-852.
632 Phillips, M.J., and G.K. Voeltz. 2016. Structure and function of ER membrane contact sites with
633 other organelles. *Nat Rev Mol Cell Biol*. 17:69-82.
634 Pizzo, P., V. Lissandron, P. Capitanio, and T. Pozzan. 2011. Ca2+ signalling in the Golgi
635 apparatus. *Cell Calcium*. 50:184-192.
636 Pizzo, P., V. Lissandron, and T. Pozzan. 2010. The trans-golgi compartment: A new distinct
637 intracellular Ca store. *Commun Integr Biol*. 3:462-464.
638 Ramazanov, B.R., M.L. Tran, and J. von Blume. 2021. Sending out molecules from the TGN.
639 *Curr Opin Cell Biol*. 71:55-62.
640 Rizzuto, R., M. Brini, M. Murgia, and T. Pozzan. 1993. Microdomains with High Ca2+ Close to
641 Ip(3)-Sensitive Channels That Are Sensed by Neighboring Mitochondria. *Science*.
642 262:744-747.
643 Rizzuto, R., P. Pinton, W. Carrington, F.S. Fay, K.E. Fogarty, L.M. Lifshitz, R.A. Tuft, and T.
644 Pozzan. 1998. Close contacts with the endoplasmic reticulum as determinants of
645 mitochondrial Ca2+ responses. *Science*. 280:1763-1766.
646 Scherer, P.E., G.Z. Lederkremer, S. Williams, M. Fogliano, G. Baldini, and H.F. Lodish. 1996.
647 Cab45, a novel (Ca2+)-binding protein localized to the Golgi lumen. *J Cell Biol*.
648 133:257-268.
649 Sepulveda, M.R., D. Marcos, M. Berrocal, L. Raeymaekers, A.M. Mata, and F. Wuytack. 2008.
650 Activity and localization of the secretory pathway Ca2+-ATPase isoform 1 (SPCA1) in
651 different areas of the mouse brain during postnatal development. *Mol Cell Neurosci*.
652 38:461-473.
653 Stalder, D., and D.C. Gershlick. 2020. Direct trafficking pathways from the Golgi apparatus to
654 the plasma membrane. *Semin Cell Dev Biol*. 107:112-125.
655 Tang, B.L. 2001. Protein trafficking mechanisms associated with neurite outgrowth and
656 polarized sorting in neurons. *J Neurochem*. 79:923-930.
657 Thillaiappan, N.B., A.P. Chavda, S.C. Tovey, D.L. Prole, and C.W. Taylor. 2017. Ca(2+) signals
658 initiate at immobile IP3 receptors adjacent to ER-plasma membrane junctions. *Nat*
659 *Commun*. 8:1505.
660 Uhlen, M., L. Fagerberg, B.M. Hallstrom, C. Lindskog, P. Oksvold, A. Mardinoglu, A.
661 Sivertsson, C. Kampf, E. Sjostedt, A. Asplund, I. Olsson, K. Edlund, E. Lundberg, S.
662 Navani, C.A. Szigyarto, J. Odeberg, D. Djureinovic, J.O. Takanen, S. Hober, T. Alm,
663 P.H. Edqvist, H. Berling, H. Tegel, J. Mulder, J. Rockberg, P. Nilsson, J.M. Schwenk, M.
664 Hamsten, K. von Feilitzen, M. Forsberg, L. Persson, F. Johansson, M. Zwahlen, G. von
665 Heijne, J. Nielsen, and F. Ponten. 2015. Proteomics. Tissue-based map of the human
666 proteome. *Science*. 347:1260419.
667 Venditti, R., M.C. Masone, and M.A. De Matteis. 2020. ER-Golgi membrane contact sites.
668 *Biochem Soc Trans*. 48:187-197.
669 Venditti, R., M.C. Masone, L.R. Rega, G. Di Tullio, M. Santoro, E. Polishchuk, I.C. Serrano,
670 V.M. Olkkonen, A. Harada, D.L. Medina, R. La Montagna, and M.A. De Matteis. 2019a.
671 The activity of Sac1 across ER-TGN contact sites requires the four-phosphate-adaptor-
672 protein-1. *J Cell Biol*. 218:783-797.
673 Venditti, R., L.R. Rega, M.C. Masone, M. Santoro, E. Polishchuk, D. Sarnataro, S. Paladino, S.
674 D'Auria, A. Varriale, V.M. Olkkonen, G. Di Tullio, R. Polishchuk, and M.A. De Matteis.

675 2019b. Molecular determinants of ER-Golgi contacts identified through a new FRET-
676 FLIM system. *J Cell Biol*. 218:1055-1065.
677 von Blume, J., A.M. Alleaume, G. Cantero-Recasens, A. Curwin, A. Carreras-Sureda, T.
678 Zimmermann, J. van Galen, Y. Wakana, M.A. Valverde, and V. Malhotra. 2011.
679 ADF/cofilin regulates secretory cargo sorting at the TGN via the Ca2+ ATPase SPCA1.
680 *Dev Cell*. 20:652-662.
681 von Blume, J., A.M. Alleaume, C. Kienzle, A. Carreras-Sureda, M. Valverde, and V. Malhotra.
682 2012. Cab45 is required for Ca(2+)-dependent secretory cargo sorting at the trans-Golgi
683 network. *J Cell Biol*. 199:1057-1066.
684 Wakana, Y., K. Hayashi, T. Nemoto, C. Watanabe, M. Taoka, J. Angulo-Capel, M.F. Garcia-
685 Parajo, H. Kumata, T. Umemura, H. Inoue, K. Arasaki, F. Campelo, and M. Tagaya.
686 2021. The ER cholesterol sensor SCAP promotes CARTS biogenesis at ER-Golgi
687 membrane contact sites. *J Cell Biol*. 220.
688 Wong, A.K.C., P. Capitanio, V. Lissandron, M. Bortolozzi, T. Pozzan, and P. Pizzo. 2013.
689 Heterogeneity of Ca-2 handling among and within Golgi compartments. *J Mol Cell Biol*.
690 5:266-276.
691 Zanetti, G., S. Prinz, S. Daum, A. Meister, R. Schekman, K. Bacia, and J.A. Briggs. 2013. The
692 structure of the COPII transport-vesicle coat assembled on membranes. *Elife*. 2:e00951.
693

694 # Figure legends
695
696 **Figure 1. Inhibition of IP3R activity delays TGN export of Cab45 clients**
697 (A) Schematic representation of the Retention Using Streptavidin Hooks (RUSH) assay with
698 fluorescent tagged client molecules. (B) Representative immunofluorescence images of the RUSH
699 experiments showing COMP-EGFP transport in HeLa lines treated with DMSO and 70 nM 2-
700 APB. HeLa cells were transfected with KDEL-IRES-SBP-COMP-EGFP and fixed at 0, 20, 40,
701 and 60 min after the addition of biotin. Z-stack images (d = 0.2 µm) were analyzed. The
702 arrowheads indicate cytoplasmic vesicles. Scale bars, 10 µm. (C) The numbers of COMP budding
703 vesicles from RUSH experiments with KDEL-IRES-SBP-COMP-EGFP in HeLa lines treated with
704 DMSO and 2-APB were quantified. The cytoplasmic vesicles were counted at each time point by
705 analyzing z-stack images (d = 0.2 µm). Scatter dot plot represents the means ± SD of at least three
706 independent experiments (n > 30 cells per condition). Statistical test, Kruskal–Wallis. (D) Plot
707 representing normalized average fluorescence intensity of COMP-EGFP in cells by FACS at 0, 60
708 and 120 minutes of RUSH experiments. (E) Plot representing normalized fluorescence intensity
709 of LyzC-EGFP within TGN (ROI was defined by GALNT1 area) in cells treated with DMSO and
710 2-APB. (F) Western blot showing LyzC-GFP in Hela cells treated with DMSO and 2-APB in cell
711 lysates and in secreted medium (top) and β-actin as a loading control.
712
713 **Figure 2. Depletion of VAPA and VAPB delays TGN export of Cab45 clients**
714 (A) Representative immunofluorescence images of RUSH experiments showing COMP-GFP
715 transport in HeLa lines treated with siRNA against VAPA and VAPB proteins. Cells were
716 transfected with KDEL-IRES-SBP-COMP-EGFP and fixed at 0, 20, 40, and 60 min after the
717 addition of biotin. Z-stack images (d = 0.2 µm) were analyzed. Scale bars, 10 µm. (B) The numbers
718 of COMP budding vesicles were quantified. The cytoplasmic vesicles were counted at each time
719 point by analyzing z-stack images (d = 0.2 µm). Scatter dot plot represents the means ± SD of at
720 least three independent experiments (n > 30 cells per condition). Statistical test, Kruskal–Wallis.
721 (C) Plot representing normalized average fluorescence intensity of COMP-EGFP in cells by FACS
722 at 0, 60 and 120 minutes of RUSH experiments in HeLa WT and VAPA/VAPB-dKO lines (D)
723 Plot representing normalized fluorescence intensity of LyzC-EGFP within TGN (ROI was defined
724 by Galnt1 area) in cells treated with non-targeting (control) siRNA and siRNA targeting VAPA
725 and VAPB. (E) Expression of VAPA and VAPB proteins in Hela WT line transfected with control
726 (non-targeting) siRNA, Hela line transfected with siVAPA/siVAPB and Hela VAPA/VAPB-dKO
727 line. β-actin was used as a loading control.
728
729 **Figure 3. MCS targeting FRET sensor responses to changes in Ca^{2+} concentration at ER-**
730 **TGN MCS**
731 (A) Schematic representation of OSBP and Twitch2b Calcium Sensor targeting Endoplasmic
732 Reticulum-Golgi membrane contact sites. The PH domain of OSBP binds to PI4P on the outer
733 leaflet of the TGN membrane, and the FFAT domain interacts with VAPA on the ER membrane.
734 (B) The calibration curve for the Twitch2b sensor used a buffer with increasing concentration of
735 free Ca^{2+} ions, demonstrating a correlation between FRET indices and free Ca^{2+}. (See Materials
736 and Methods for a detailed description). (C) Pseudocolor map of FRET index and dot plot (D)
737 representing FRET indices for PH-FFAT-Twitch2b and PH-FFAT-Twitch9x within Golgi ROI of
738 live cells and at steady state (***p<0.05). (E) Pseudocolor map of FRET index and dot plot (F)
739 representing FRET indices for PH-FFAT-Twitch2b at steady state and treated with 25uM BAPTA-

740 AM for 20 min (***p<0.05). (G) Pseudocolor map of FRET index and dot plot (H) representing
741 FRET indices for PH-FFAT-Twitch2b at steady state and treated with 1uM ionomycin for 20 min
742 (***p<0.05). (I) Pseudocolor map of FRET index and dot plot (J) representing FRET indices for
743 PH-FFAT-Twitch2b at steady state and treated with 1uM Histamine for 2 min (***p<0.05).
744 Pseudocolor bar FRET index value in range 0-0.4.
745
746 **Figure 4. Ca^{2+} flux at ER-TGN MCS is coupled to protein trafficking**
747 (A) Schematic representation of experiment and effect on protein trafficking in live cells during
748 20°C block and cycloheximide (CHX) treatment. (B) Pseudocolor maps of FRET index for PH-
749 FFAT-Twitch2b within Golgi ROI of live cells at described above conditions. Pseudocolor bar
750 FRET index value in range 0-0.4. (C) Dot plot representing FRET index for PH-FFAT-Twitch2b
751 at steady state, after 20°C block for 1 and 2 hours and after 10 min recovery at 37°C (***p<0.05).
752 (D) Dot plot representing FRET index for PH-FFAT-Twitch2b at steady state, treated with CHX
753 for 1, 2, 4 hours and after 1 h 20°C block. (***p<0.05), (E) Dot plot representing normalized FRET
754 index for PH-FFAT-Twitch2b at steady state, after 1 h 20°C block and effect of ionomycin at 37°C
755 and 20°C conditions (***p<0.05).
756
757 **Figure 5. The model depicting the role of contact sites and IP3R-dependent release of**
758 **Calcium ions for SPCA1-dependent sorting at TGN**
759

Supplementary data

Supplementary Figure legends

Supplementary 1. RUSH experiments using Cab45 clients demonstrate that delay in protein trafficking takes place at TGN

(A) Representative histograms plotting fluorescence intensity distribution of COMP-GFP in cells at 30, 60, and 120 minutes (shown in red) during the RUSH experiment compared to timepoint "0" (shown in green overlay) in HeLa WT cells line treated with DMSO (upper row), HeLa WT cells treated with 2-APB (middle row), and HeLa VAPA/VAPB-dKO line (bottom row). 10.000 cells were analyzed for each condition. (B) Graph depicting mean normalized fluorescence intensity (F.I.) of RUSH LyzC-EGFP in BFP-GALNT1 (Golgi marker) region of interest (ROI) from and after the time when the maximal LyzC-EGFP F.I. is reached in the ROI (peak Golgi F.I.). The decrease in LyzC-EGFP F.I. represents the Golgi exit in the HeLa line treated with DMSO (black) versus 2-APB treated (red). At least 10 cells from independent experiments for each condition were analyzed with nonlinear regression (exponential function) indicated in the plot using GraphPad Prism9 built-in regression. (C) Graph depicting mean normalized fluorescence intensity (F.I.) of RUSH LyzC-EGFP in BFP-GALNT1 (Golgi marker) region of interest (ROI) from and after the time when the maximal LyzC-EGFP F.I. is reached in the ROI (peak Golgi F.I.). The decrease in LyzC-EGFP F.I. represents the Golgi exit in the HeLa line transfected with control siRNA (black) versus the Hela line transfected with siRNA to VAPA and VAPB (red). At least 10 cells from independent experiments for each condition were analyzed with nonlinear regression (exponential function) indicated in the plot using GraphPad Prism9 built-in regression.

Supplementary 2. VAPA/VAPB dKO HeLa lines demonstrate delay in TGN export of Cab45 clients in RUSH experiments

(A) Representative immunofluorescence images of RUSH experiments showing LyzC-GFP transport in HeLa WT and VAPA/B-dKO cell lines. Cells were transfected with KDEL-IRES-SBP-LyzC-EGFP and fixed at 0, 20, 40, and 60 min after adding biotin. Z-stack images (d = 0.2 µm) were analyzed. The arrowheads indicate cytoplasmic vesicles. Scale bars, 10 µm. (B) Representative immunofluorescence images of RUSH experiments showing COMP-GFP transport in HeLa WT and VAPA/B-dKO cell lines. Cells were transfected with KDEL-IRES-SBP-COMP-EGFP and fixed at 0, 20, 40, and 60 min after adding biotin. Z-stack images (d = 0.2 µm) were analyzed. The arrowheads indicate cytoplasmic vesicles. Scale bars, 10 µm. (C) The numbers of LyzC budding vesicles were quantified. The cytoplasmic vesicles were counted at each time point by analyzing z-stack images (d = 0.2 µm). The scatter dot plot represents the means ± SD of at least three independent experiments (n > 30 cells per condition). Statistical test, Kruskal–Wallis. (D) The numbers of COMP budding vesicles were quantified. The cytoplasmic vesicles were counted at each time point by analyzing z-stack images (d = 0.2 µm). The scatter dot plot represents the means ± SD of at least three independent experiments (n > 30 cells per condition). Statistical test, Kruskal–Wallis.

Supplementary 3. MCS targeting FRET sensors localize with TGN markers.

(A) Schematic representation of the domain structure of OSBP (top construct) and Twitch sensors fused proteins targeting ER-Golgi contact sites (N-PH-FFAT-Twitch and PH-FFAT-Twitch) as well as sensors targeting ER (fused with VAPA protein) and cytoplasmic version (two bottom

806 constructs) used in this study. (B) IF images of HeLa lines stably expressing Twitch2b sensor
807 targeting cytoplasm, ER and ER-TGN contact sites. (C) IF images of HeLa line expressing
808 Twitch2b sensor targeting ER-TGN contact sites and its localization compared to TGN46 (TGN
809 marker). (D) IF images of HeLa line expressing Twitch2b sensor targeting ER-TGN contact sites
810 and its localization compared to GM130 (cis Golgi marker). (E) Dot plot representing FRET index
811 for PH-FFAT-Twitch2b and PH-FFAT-Twitch7x, PH-FFAT-Twitch8x and PH-FFAT-Twitch9x
812 within Golgi ROI of live cells and at steady state (***$p<0.05$); (F) Dot plot representing FRET
813 index for PH-FFAT-Twitch2b and N-PH-FFAT-Twotch2b in cells at steady state. (G) Dot plot
814 representing FRET index for N-PH-FFAT-Twitch2b cells at steady state and treated with 1uM
815 ionomycin for 20 min (***$p<0.05$). (H) Dot plot representing FRET index for N-PH-FFAT-
816 Twitch2b cells at steady state and treated with 1uM Histamine for 2 min(***$p<0.05$).
817
818 **Supplementary 4. Calibration procedures of Twitch2b sensor and fluorescence channels for**
819 **FRET experiments**
820 (A) Schematic representation of the calibration experiment of Twich2b calcium sensor using Ca-
821 EGTA buffers in live cells (Please see Materials and Methods section for detailed description). (B)
822 Pseudocolor heatmap of FRET index for CYTO-Twitch2b during calibration experiment.
823 Pseudocolor bar FRET index value in range 0-0.4. (C) Calibration of fluorescence channels for
824 Twitch sensor using HeLa lines expressing PH-FFAT-mCerulean3 (only FRET donor), HeLa lines
825 expressing PH-FFAT-cpVenus (only FRET acceptor)) and PH-FFAT-Twitch2b (FRET pair with
826 calcium binding domain) sensor.
827
828
829
830 **Table legends**
831
832 Supplementary Table1. Twitch sensors and their affinity to Ca^{2+} ions.

FRET Sensor	**Calcium affinity of TnC (KD)**
Twitch 2b	200 nM
Twitch 7x	51.5 uM
Twitch 8x	139 uM
Twitch 9x	174 uM

833
834
835 Supplementary Table2. Twitch sensors and aminoacidic sequences of calcium-binding domain

FRET Sensor	**Aminoacidic sequence of Calcium binding domain of Twitch sensors**
Twitch 2b	MQVADASEEELSECFRIFDFDGN_GFIDREEFGDIIRLTGE QLTDEDVDEIFGDSDTDKN_GRIDFDEFLKMVENVQPIYP
Twitch 7x	MQVADASEEELSECFRIFDFDGNDGFIDREEFGDIIRLTGE QLTDEDVDEIFGDSDTDKN_GRIDFDEFLKMVENVQPIYP

Twitch 8x	MQVADASEEELSECFRIFDFDGN_GFIDREEFGDIIRLTGE QLTDEDVDEIFGDSDTDKNSGRIDFDEFLKMVENVQPIYP
Twitch 9x	MQ__DASEEELSECFRIFDKDGNDGFIDREEFGDIIRLTGE QLTDEDVDEIFGDSDTDKN_GRIDFDEFLKMVENVQPIYP

836

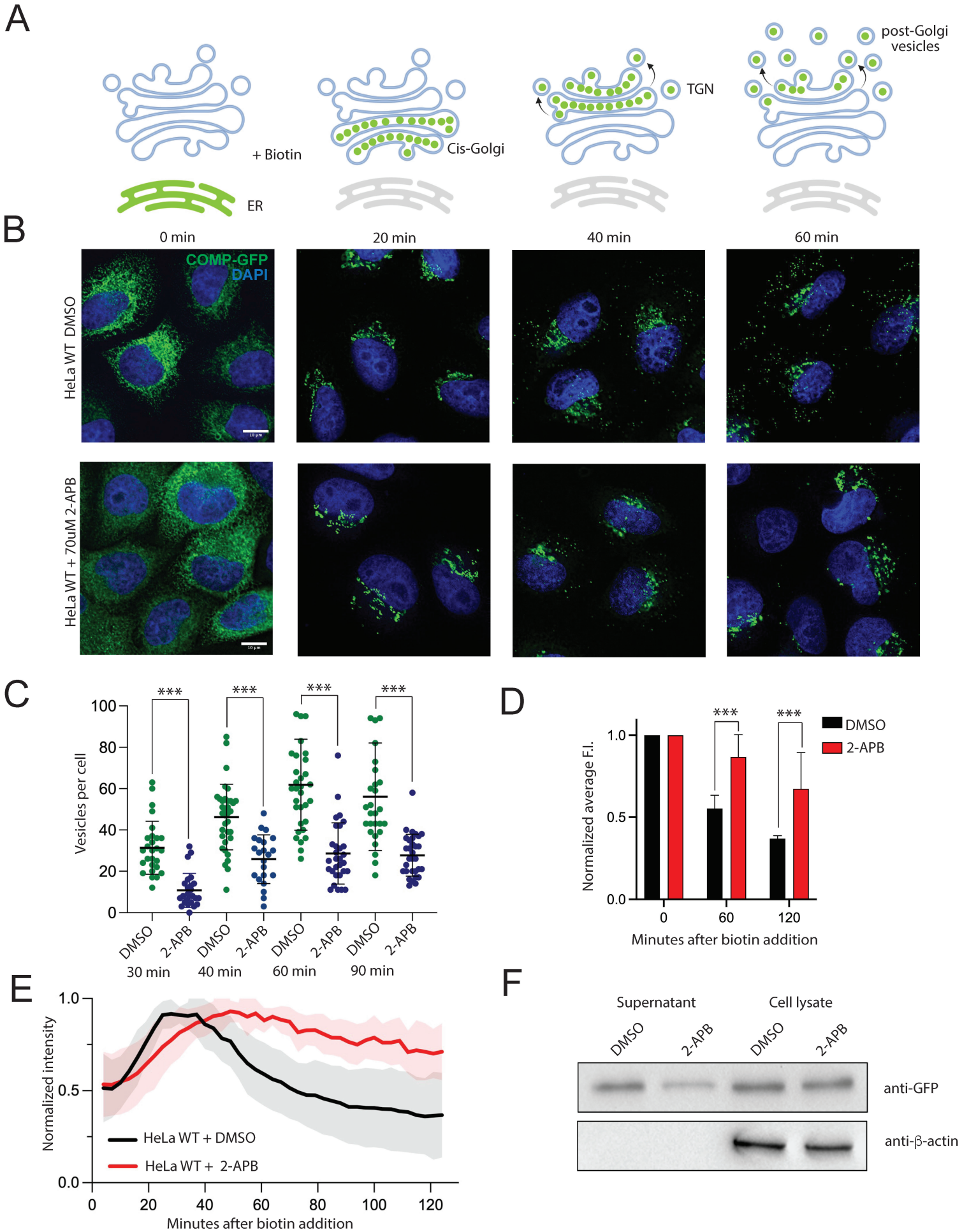

Figure 1. Inhibition of IP3R activity delays TGN export of Cab45 clients
(A) Schematic representation of the Retention Using Streptavidin Hooks (RUSH) assay with fluorescent tagged client molecules. (B) Representative immunofluorescence images of the RUSH experiments showing COMP-EGFP transport in HeLa lines treated with DMSO and 70 nM 2-APB. HeLa cells were transfected with KDEL-IRES-SBP-COMP-EGFP and fixed at 0, 20, 40, and 60 min after the addition of biotin. Z-stack images (d = 0.2 μm) were analyzed. The arrowheads indicate cytoplasmic vesicles. Scale bars, 10 μm. (C) The numbers of COMP budding vesicles from RUSH experiments with KDEL-IRES-SBP-COMP-EGFP in HeLa lines treated with DMSO and 2-APB were quantified. The cytoplasmic vesicles were counted at each time point by analyzing z-stack images (d = 0.2 μm). Scatter dot plot represents the means ± SD of at least three independent experiments (n > 30 cells per condition). Statistical test, Kruskal–Wallis. (D) Plot representing normalized average fluorescence intensity (F.I.) of COMP-EGFP in cells by FACS at 0, 60 and 120 minutes of RUSH experiments, ***p<0.001 (E) Plot representing normalized fluorescence intensity of LyzC-EGFP within TGN (ROI was defined by GALNT1 area) in cells treated with DMSO and 2-APB. (F) Western blot showing LyzC-GFP in Hela cells treated with DMSO and 2-APB in cell lysates and in secreted medium (top) and β-actin as a loading control.

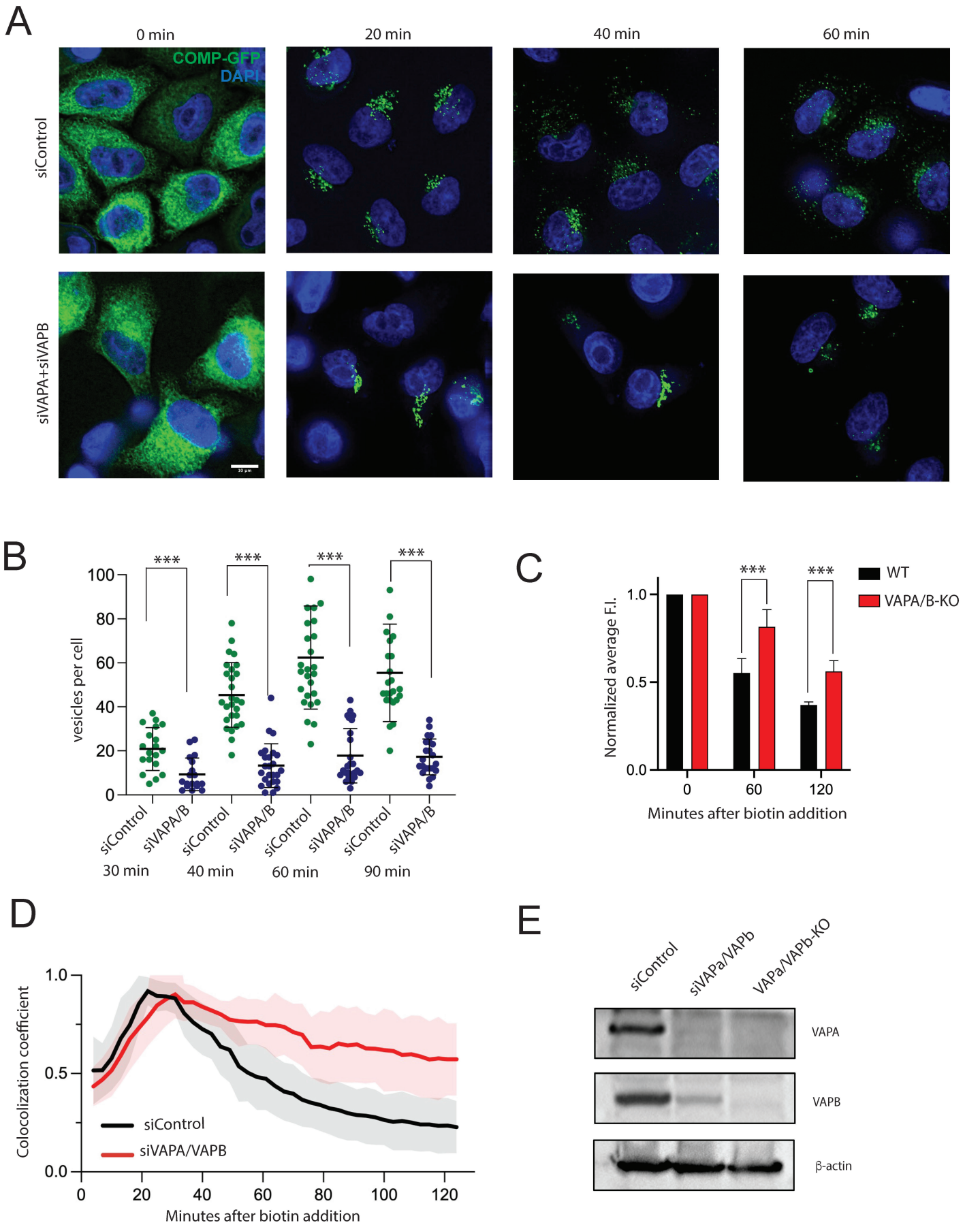

Figure 2. Depletion of VAPA and VAPB delays TGN export of Cab45 clients
(A) Representative immunofluorescence images of RUSH experiments showing COMP-GFP transport in HeLa lines treated with siRNA against VAPA and VAPB proteins. Cells were transfected with KDEL-IRES-SBP-COMP-EGFP and fixed at 0, 20, 40, and 60 min after the addition of biotin. Z-stack images (d = 0.2 μm) were analyzed. Scale bars, 10 μm. (B) The numbers of COMP budding vesicles were quantified. The cytoplasmic vesicles were counted at each time point by analyzing z-stack images (d = 0.2 μm). Scatter dot plot represents the means ± SD of at least three independent experiments (n > 30 cells per condition). Statistical test, Kruskal–Wallis. (C) Plot representing normalized average fluorescence intensity (F.I.) of COMP-EGFP in cells by FACS at 0, 60 and 120 minutes of RUSH experiments in HeLa WT and VAPA/VAPB-dKO lines, ***p<0.001; (D) Plot representing normalized fluorescence intensity of LyzC-EGFP within TGN (ROI was defined by GalNt1 area) in cells treated with non-targeting (control) siRNA and siRNA targeting VAPA and VAPB. (E) Expression of VAPA and VAPB proteins in Hela WT line transfected with control (non-targeting) siRNA, Hela line transfected with siVAPA/siVAPB and Hela VAPA/VAPB-dKO line. β-actin was used as a loading control.

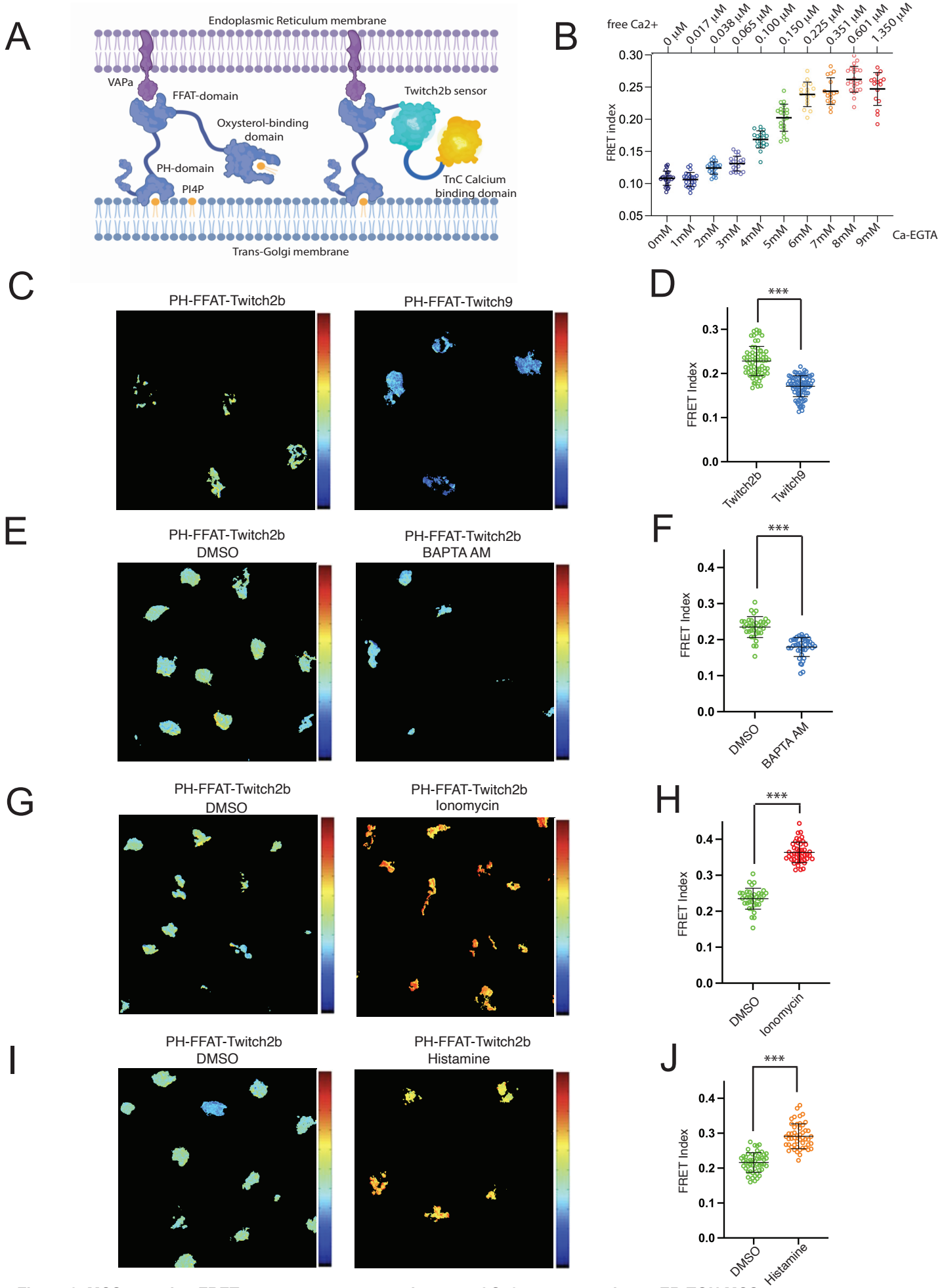

Figure 3. MCS targeting FRET sensor responses to changes of Ca2+ concentration at ER-TGN MCS.
(A) Schematic representation of OSBP and Twitch2b Calcium Sensor targeting Endoplasmic Reticulum-Golgi membrane contact sites. PH domain of OSBP binds to PI4P on the outer leaflet of the TGN membrane and FFAT domain interacts with VAPA on the ER membrane. (B) Calibration curve for Twitch2b sensor performed used buffer with increasing concentration of free Ca2+ ions demonstrating correlation between FRET indices and free Ca2+. (See Materials and Methods for a detailed description). (C) Pseudocolor map of FRET index and dot plot (D) representing FRET indices for PH-FFAT-Twitch2b and PH-FFAT-Twitch9x within Golgi ROI of live cells and at steady state (***p<0.05). (E) Pseudocolor map of FRET index and dot plot (F) representing FRET indices for PH-FFAT-Twitch2b at steady state and treated with 25uM BAPTA-AM for 20 min (***p<0.05). (G) Pseudocolor map of FRET index and dot plot (H) representing FRET indices for PH-FFAT-Twitch2b at steady state and treated with 1uM ionomycin for 20 min (***p<0.05). (I) Pseudocolor map of FRET index and dot plot (J) representing FRET indices for PH-FFAT-Twitch2b at steady state and treated with 1uM Histamine for 2 min (***p<0.05). Pseudocolor bar FRET index value in range 0-0.4.

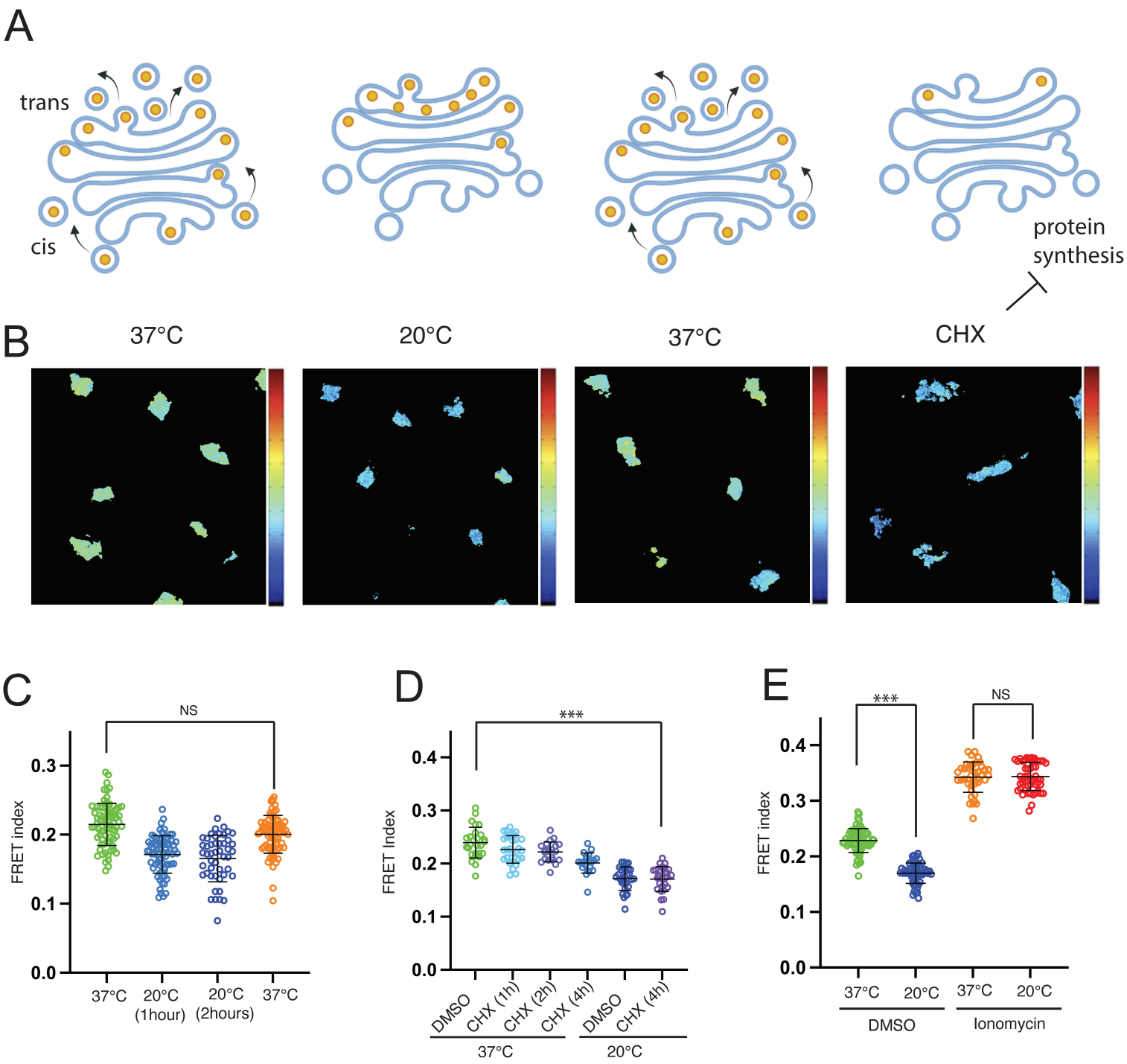

Figure 4. Ca2+ flux at ER-TGN MCS is coupled to protein trafficking
(A) Schematic representation of experiment and effect on protein trafficking in live cells during 20°C block and cycloheximide (CHX) treatment. (B) Pseudocolor maps of FRET index for PH-FFAT-Twitch2b within Golgi ROI of live cells at described above conditions. Pseudocolor bar FRET index value in range 0-0.4. (C) Dot plot representing FRET index for PH-FFAT-Twitch2b at steady state, after 20°C block for 1 and 2 hours and after 10 min recovery at 37°C (***p<0.05). (D) Dot plot representing FRET index for PH-FFAT-Twitch2b at steady state, treated with CHX for 1, 2, 4 hours and after 1h 20°C block. (***p<0.05), (E) Dot plot representing normalized FRET index for PH-FFAT-Twitch2b at steady state, after 1h 20°C block and effect of ionomycin at 37°C and 20°C conditions (***p<0.05).

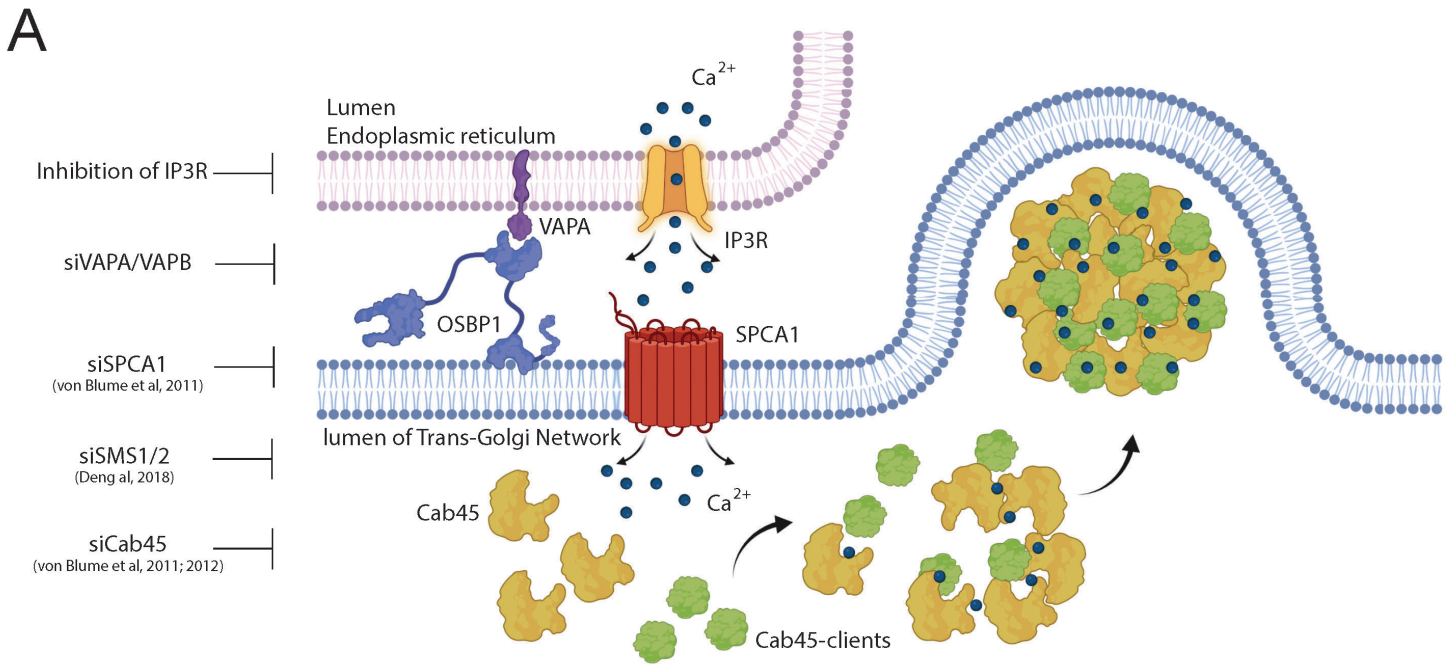

Figure 5A. The model depicting the role of contact sites and IP3R-dependent release of Calcium ions for SPCA1 dependent sorting at TGN.